4. Perspective

Recent advances in imaging techniques allow for anatomical analyses of human embryo specimens in earlier stages and for clinical prenatal diagnosis during the first trimester. Current information on normal development during embryonic stages, however, remains insufficient to achieve such clinical evaluation. Further investigations are critical to gain insight into the dynamic and complex events occurring during organogenesis. Dynamic modeling of embryonic structures and 3D digital reconstructions will be valuable tools to elucidate the complex anatomical changes taking place during early embryonic stages. They will serve as useful references to evaluate the appropriate development of embryonic organs, and understand how adjacent organs affect each other's morphology. Now and in the future, this type of information will be indispensable to researchers and to clinicians, and more particularly in respect to the obstetrical ultrasonography conducted in the early gestational weeks.

5. Appendix (softwares)

The use of software is necessary for reconstruction into 3D images and morphometric analysis. The software programs used in this chapter are summarized below. More information is available on the URL of their respective websites.

5.1 OsiriX (http://www.osirix-viewer.com/index.html)

OsiriX is an image processing software dedicated to DICOM images produced by imaging equipment (e.g. MRI, CT, PET, PET-CT, SPECT-CT, Ultrasounds). It is fully compliant with the DICOM standard for image communication and image file formats. OsiriX is able to receive images transferred by DICOM communication protocol from any PACS or imaging modality.

5.2 Image J (http://rsbweb.nih.gov/ij/index.html)

ImageJ is a public domain Java image-processing program inspired from the NIH Image software developed for Macintosh. It runs, either as an online applet or as a downloadable application, on any computer with a Java 1.4 or later virtual machine.

5.3 Delta viewer (http://delta.math.sci.osaka-u.ac.jp/DeltaViewer/index.html)

DeltaViewer is an application program developed for Apple Macintosh. DeltaViewer reads sequences of cross-sectional images of a sample in a manner similar to confocal laser microscopes, CT, MRI, optical or electron microscopes. The computer program then reconstructs the surface of the scanned sample, and displays the image on the screen. The image can then be freely rotated, for characterization of 3D shapes and spatial relationships.

5.4 Avizo (http://www.vsg3d.com/avizo/overview)

Avizo® software is a powerful, multifaceted tool for visualizing, manipulating, and understanding scientific and industrial data. Wherever 3D data sets need to be processed, in materials science, geosciences, environmental or engineering applications, Avizo offers abundant state-of-the-art features within an intuitive workflow and easy-to-use graphical user interfaces.

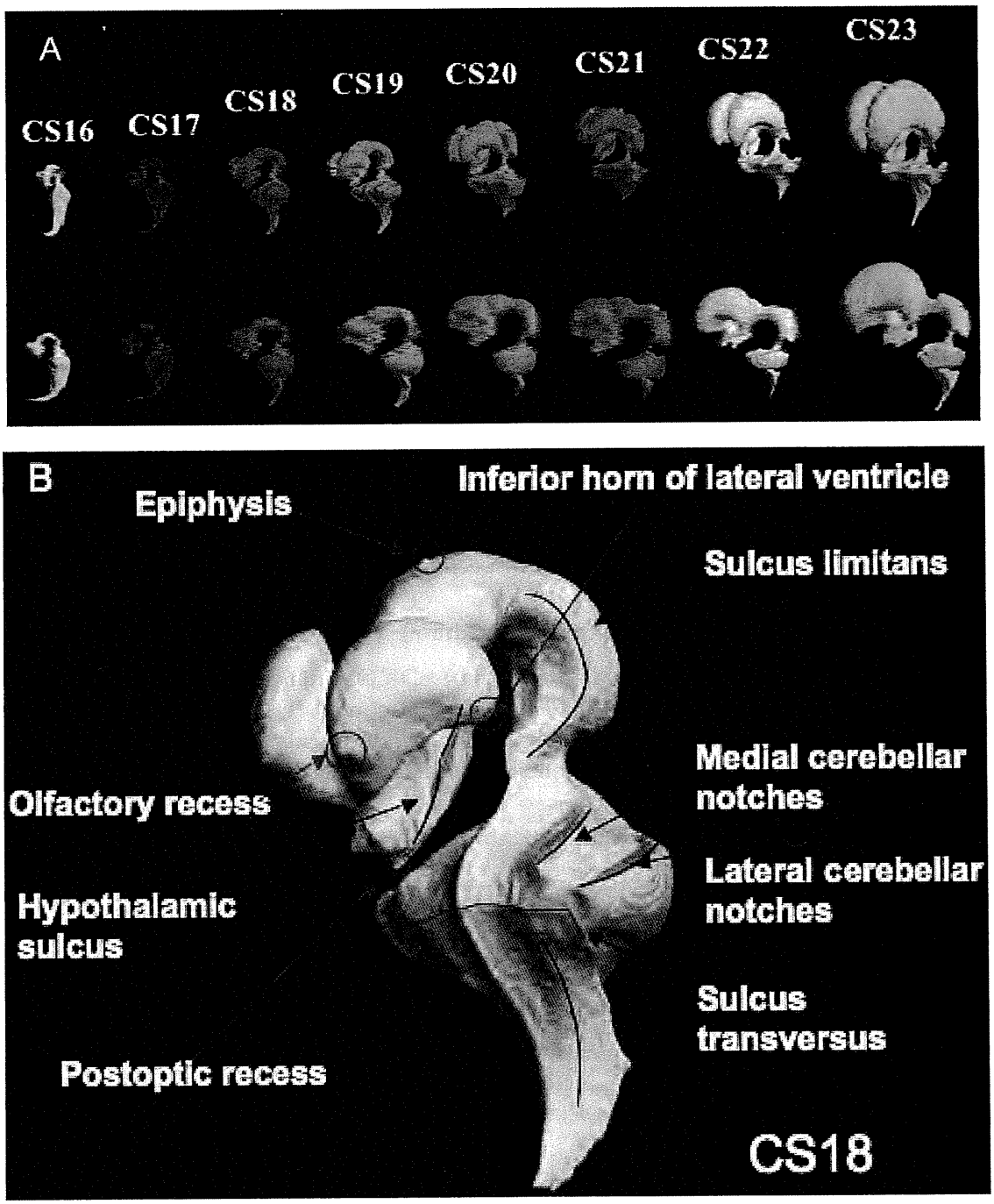

Fig. 8. (A) Representative 3D images of cerebral ventricles between Carnegie stage 16 and stage 23. (B) 3D image illustrating the conservation of anatomic landmarks.

5.5 FMRIB Software Library (FSL) (http://www.fmrib.ox.ac.uk/fsl/index.html)

FSL is a comprehensive library of analytical tools for fMRI (functional magnetic resonance imaging), MRI and DTI (Diffusion tensor imaging) brain imaging data. FSL was mainly

developed by members of the Analysis Group at the FMRIB, Oxford, UK. FSL runs on Apple and PCs (Linux and Windows), and is easy to install. Most of the tools can be run either from the command line or as "point-and-click" graphical user interfaces.

5.6 Analyze (http://www.mayo.edu/bir/Software/Analyze/Analyze.html)

Analyze 10.0 is a powerful, comprehensive software package for multi-dimensional display, processing, and measurement of multi-modality biomedical images. Product of more than 25 years of biomedical imaging research and development at Mayo Clinic, this integrated, total solution allows you to significantly enhance your multidimensional biomedical imaging productivity.

6. Acknowledgments

We would like to thank Ms Merumo Ueda, Ms Nami Uematsu, Ms Kyoko Nakajima, and Ms Sayuri Nunomura at the Kyoto University Graduate School of Medicine, Human Health Science, for conducting some of the experiments; Ms Chigako Uwabe at the Congenital Anomaly Research Center for technical assistance in handling human embryos; Prof. Masaaki Wada at the Graduate School of Information Science and Technology at Osaka University for help on the use of the DeltaViewer software; Prof. Katsumi Kose and Dr. Yoshimasa Matsuda at the Institute of Applied Physics at University of Tsukuba and Dr. Stasia A Anderson at the NHLBI Animal MRI Core, National Institutes of Health, for technical help with MR imaging; and Prof. Kohei Shiota, Vice President of Kyoto University, for his support and guidance on the project. The researches were financially supported by Grants #228073, #238058, #21790810 and #22591199 from the Japan Society for the Promotion of Science (JSPS) and the Japan Science and Technology (JST) institute for Bioinformatics Research and Development (BIRD). The researches were also supported by Japan Spina Bifida and Hydrocephalus Research Foundation, and Konica Minolta Science and Technology Foundation. The studies presented in this chapter were approved by the Medical Ethics Committee at Kyoto University Graduate School of Medicine (Kyoto, Japan).

7. References

Becker, B. P. & Bonse, U. 1974. The skew-symmetric two-crystal X-ray interferometer. *Journal of Applied Crystallography,* 7, 593-598.

Bone, S. N., Johnson, G. A. & Thompson, M. B. 1986. Three-dimensional magnetic resonance microscopy of the developing chick embryo. *Invest Radiol,* 21, 782-7.

Born, G. 1883. Die Plattenmodelliermethode. *Archiv für mikroskopische Anatomie.* 22, 584-99.

Effmann, E. L., Johnson, G. A., Smith, B. R., Talbott, G. A. & Cofer, G. 1988. Magnetic resonance microscopy of chick embryos in ovo. *Teratology,* 38, 59-65.

Haishi, T., Uematsu, T., Matsuda, Y. & Kose, K. 2001. Development of a 1.0 T MR microscope using a Nd-Fe-B permanent magnet. *Magnetic resonance imaging,* 19, 875-80.

Heard, O. O. 1951. Section compression photographically rectified. *The Anatomical record,* 109, 745-55.

Heard, O. O. 1953. The influence of surface forces in microtomy. *The Anatomical record,* 117, 725-39.

Heard, O. O. 1957. Methods used by C.H. Heuser in preparing and sectioning early embryos. *Contributions to Embryology,* 36, 1-18.

Matsuda, Y., Ono, S., Otake, Y., Handa, S., Kose, K., Haishi, T., Yamada, S., Uwabe, C. & Shiota, K. 2007. Imaging of a large collection of human embryo using a super-parallel MR microscope. *Magnetic resonance in medical sciences : MRMS : an official journal of Japan Society of Magnetic Resonance.* 6, 139-46.

Matsuda, Y., Utsuzawa, S., Kurimoto, T., Haishi, T., Yamazaki, Y., Kose, K., Anno, I. & Marutani, M. 2003. Super-parallel MR microscope. *Magnetic resonance in medicine : official journal of the Society of Magnetic Resonance in Medicine / Society of Magnetic Resonance in Medicine.* 50, 183-9.

Momose, A. & Fukuda, J. 1995. Phase-contrast radiographs of nonstained rat cerebellar specimen. *Medical physics,* 22, 375-9.

Momose, A., Takeda, T., Itai, Y. & Hirano, K. 1996. Phase-contrast X-ray computed tomography for observing biological soft tissues. *Nature medicine.* 2, 473-5.

Nakashima, T., Hirose, A., Yamada, S., Uwabe, C., Kose, K. & Takakuwa, T. 2011. Morphometric analysis of the brain vesicles during the human embryonic period by magnetic resonance microscopic imaging. Congenital Anomalies. doi: 10.1111/j.1741-4520.2011.00345.x

Nishimura, H. 1975. Prenatal versus postnatal malformations based on the Japanese experience on induced abortions in the human being. . *In:* BLANDEU, R. (ed.) *Aging Gamates.* Basel: S. Karger AG.

Nishimura, H., Takano, K., Tanimura, T. & Yasuda, M. 1968. Normal and abnormal development of human embryos: first report of the analysis of 1,213 intact embryos. *Teratology,* 1, 281-90.

O'Rahilly, R. 1988. One Hundred Years of Human Embryology. *In:* KALTER, H. (ed.) *Issues and Reviews in Terratology* New York: Plenum Press.

O'Rahilly, R. & Müller, F. 1987. *Developmental stages in human embryos: including a revision of Streeter's "horizons" and a survey of the Carnegie Collection.,* Washington, DC, Carnegie Institution of Washington Publication.

Rohlf, F. J. & Bookstein, F. L. 1990. *Proceedings Of The Michigan Morphometrics Workshop,* Ann Arbor, MI, University of Michigan Museum of Zoology.

Rosenthal, J., Mangal, V., Walker, D., Bennett, M., Mohun, T. J. & Lo, C. W. 2004. Rapid high resolution three dimensional reconstruction of embryos with episcopic fluorescence image capture. *Birth defects research. Part C, Embryo today : reviews,* 72, 213-23.

Shiota, K. 1991. Development and intrauterine fate of normal and abnormal human conceptuses. *Congenital Anomalies,* 31, 67-80.

Shiota, K., Yamada, S., Nakatsu-Komatsu, T., Uwabe, C., Kose, K., Matsuda, Y., Haishi, T., Mizuta, S. & Matsuda, T. 2007. Visualization of human prenatal development by magnetic resonance imaging (MRI). *American journal of medical genetics. Part A,* 143A, 3121-6.

Smith, B. R. 1999. Visualizing human embryos. *Scientific American,* 280, 76-81.

Smith, B. R. 2000. Magnetic resonance imaging analysis of embryos. *Methods in molecular biology,* 135, 211-6.

Smith, B. R. 2001. Magnetic resonance microscopy in cardiac development. *Microscopy research and technique,* 52, 323-30.

Smith, B. R., Effmann, E. L. & Johnson, G. A. 1992. MR microscopy of chick embryo vasculature. *Journal of magnetic resonance imaging: JMRI.* 2, 237-40.

Smith, B. R., Huff, D. S. & Johnson, G. A. 1999. Magnetic resonance imaging of embryos: an Internet resource for the study of embryonic development. *Computerized medical imaging and graphics : the official journal of the Computerized Medical Imaging Society,* 23, 33-40.

Smith, B. R., Johnson, G. A., Groman, E. V. & Linney, E. 1994. Magnetic resonance microscopy of mouse embryos. *Proc Natl Acad Sci U S A,* 91, 3530-3.

Smith, B. R., Linney, E., Huff, D. S. & Johnson, G. A. 1996. Magnetic resonance microscopy of embryos. *Computerized medical imaging and graphics: the official journal of the Computerized Medical Imaging Society.* 20, 483-90.

Weninger, W. J., Geyer, S. H., Mohun, T. J., Rasskin-Gutman, D., Matsui, T., Ribeiro, I., Costa Lda, F., Izpisua-Belmonte, J. C. & Muller, G. B. 2006. High-resolution episcopic microscopy: a rapid technique for high detailed 3D analysis of gene activity in the context of tissue architecture and morphology. *Anatomy and embryology,* 211, 213-21.

Weninger, W. J. & Mohun, T. 2002. Phenotyping transgenic embryos: a rapid 3-D screening method based on episcopic fluorescence image capturing. *Nature genetics,* 30, 59-65.

Yamada, S., Itoh, H., Uwabe, C., Fujihara, S., Nishibori, C., Wada, M., Fujii, S. & Shiota, K. 2007. Computerized three-dimensional analysis of the heart and great vessels in normal and holoprosencephalic human embryos. *Anatomical record : advances in integrative anatomy and evolutionary biology,* 290, 259-67.

Yamada, S., Samtani, R. R., Lee, E. S., Lockett, E., Uwabe, C., Shiota, K., Anderson, S. A. & Lo, C. W. 2010. Developmental atlas of the early first trimester human embryo. *Developmental dynamics : an official publication of the American Association of Anatomists,* 239, 1585-95.

Yamada, S., Uwabe, C., Fujii, S. & Shiota, K. 2004. Phenotypic variability in human embryonic holoprosencephaly in the Kyoto Collection. *Birth Defects Res A Clin Mol Teratol,* 70, 495-508.

Yamada, S., Uwabe, C., Nakatsu-Komatsu, T., Minekura, Y., Iwakura, M., Motoki, T., Nishimiya, K., Iiyama, M., Kakusho, K., Minoh, M., Mizuta, S., Matsuda, T., Matsuda, Y., Haishi, T., Kose, K., Fujii, S. & Shiota, K. 2006. Graphic and movie illustrations of human prenatal development and their application to embryological education based on the human embryo specimens in the Kyoto collection. *Developmental dynamics : an official publication of the American Association of Anatomists,* 235, 468-77.

Yoneyama, A., Takeda, T., Tsuchiya, Y., Wu, J., Lwin, T. T., Koizumi, A., Hyodo, K. & Itai, Y. 2004. A phase-contrast X-ray imaging system—with a 60×30 mm field of view—based on a skew-symmetric two-crystal X-ray inteferometer. *Nuclear Instruments and Methods in Physics Research Section A: Accelerators, Spectrometers, Detectors and Associated Equipment,* 523, 217-222.

Yoneyama, A., Yamada, S. & Takeda, T. 2011. Fine Biomedical Imaging Using X-Ray Phase-Sensitive Technique. *In:* Gargiulo, D. G., Mcewan, A. (ed.) *Advanced Biomedical Engineering*. InTech. p107-128.

THE ANATOMICAL RECORD 295:51–59 (2012)

Embryonic Liver Morphology and Morphometry by Magnetic Resonance Microscopic Imaging

AYUMI HIROSE,[1] TAKASHI NAKASHIMA,[1] SHIGEHITO YAMADA,[2] CHIGAKO UWABE,[2] KATSUMI KOSE,[3] AND TETSUYA TAKAKUWA[1]*

[1]Human Health Science, Graduate School of Medicine, Kyoto University Kyoto, Japan
[2]Congenital Anomaly Research Center, Kyoto University Graduate School of Medicine, Kyoto, Japan
[3]Institute of Applied Physics, University of Tsukuba, Ibaragi, Japan

ABSTRACT

Embryonic liver has a unique external morphology and quantitative morphometry, based on magnetic resonance imaging data of human embryos from the Kyoto Collection of Human Embryos. Liver morphogenesis is strongly affected by the adjacent organs and tissues. The left ventricle develops to the left medial-caudal side, which results in the formation of a depression at left medial region and a prominence bilaterally at the cranial surface of the liver between Carnegie Stage (CS)17 and CS19. An imprint of the stomach that formed at the dorsal left-medial region of the liver became more marked with development until CS23. A depression induced by the umbilicus formed at the ventral region of the liver between CS16 and CS19. An indentation caused by the right adrenal gland formed at the dorsal-caudal region of the liver surface from CS20. Morphometric analysis revealed that the volume of the liver increased exponentially from CS14 through CS23. The liver developed preferentially along the dorsoventral axis and right/left axis until CS17, along the craniocaudal axis between CS17 and CS19, and then in all directions after CS19. Several important developmental phenomena, such as differentiation of the diaphragm, the extension of the body axis of the embryo, and the physiologic herniation of the intestine into the umbilical cord, may affect morphometric data. These data contribute to a better understanding of liver development as well as the morphogenesis of adjacent organs, both temporally and spatially, and serve as a useful reference for fetal medicine and prenatal diagnosis. Anat Rec, 295:51–59, 2012. © 2011 Wiley Periodicals, Inc.

Key words: liver morphology; morphometry; human embryo; magnetic resonance imaging

Additional Supporting Information may be found in the online version of this article.

Abbreviations used: 3D = three-dimensional; CS = Carnegie stages; HV = hepatic veins; IVC = inferior vena cava; L_{CC} = craniocaudal length; L_{DV} = dorsoventral length; L_{TH} = trunk height; L_{TR} = transverse length; MR = magnetic resonance; ROI = region of interest.

Grant sponsor: Japan Society for the Promotion of Science, BIRD of Japan Science and Technology Agency (JST); Grant numbers: 22591199, 228073, 238058, 21790180.

*Correspondence to: Dr. Tetsuya Takakuwa, Human Health Science, Graduate School of Medicine, Kyoto University, 606-8507 Sakyo-ku Shogoin Kawahara-cyo 53, Kyoto, Japan.
E-mail: tez@hs.med.kyoto-u.ac.jp

Received 11 March 2011; Accepted 5 September 2011
DOI 10.1002/ar.21496
Published online 18 November 2011 in Wiley Online Library (wileyonlinelibrary.com).

The liver occupies a large space in the abdominal cavity during most of the prenatal period and plays an important role in the development of functional organs (Lemaigre, 2009; Sadler and Langman, 2010). The liver becomes a hematopoietic organ after 6 weeks (Drews, 1995) and begins to metabolize important biochemical materials for development, such as albumin, bile, glycogen, and fetal-specific proteins, at around 8 weeks (Carlson, 2009).

The development of the liver proceeds in a unique manner. The liver develops at Carnegie Stage (CS) 11 (30 days after fertilization) as an outgrowth of the endodermal epithelium, the liver bud, from the caudal part of the foregut. The liver originates from two different tissues: angioblastic tissue from the coelomic surface cells and epithelial columns sprouting from the hepatic evagination of the gut epithelium (O'Rahilly and Müller, 1987). The liver lies at an active center of angiogenesis in the early embryonic period. The asymmetricity of the afferent venous vessels of the liver derives from two specific circulation systems: the vitelline and umbilical veins, which are acquired between CS13 and CS16 (Mall, 1906; Dickson, 1957; Collardeau-Frachon and Scoazec, 2008). Efferent venous vessels, including the right, left, and middle hepatic veins (HVs) and the inferior vena cava (IVC), form at similar stages. The developmental process of the efferent venous vessels is not as well studied as that of the afferent venous vessels (Mall, 1906; Dickson, 1957; Couinaud, 1996; Collardeau-Frachon and Scoazec, 2008).

Among recent three-dimensional (3D) imaging techniques, magnetic resonance (MR) microscopy is a powerful tool for 3D measurements. It is a noninvasive and nondestructive imaging method, and has been applied to analyze embryonic development in different animal models (Bone et al., 1986; Smith et al., 1992, 1994, 1996). MR imaging of embryos is highly advantageous (Effmann et al., 1988; Smith et al., 1992; Haishi et al., 2001), providing a resolution of 40 μm/pixel or better with long scan times. Kyoto and Tsukuba Universities began a project in 1999 to acquire 3D MR microscopic images of thousands of human embryos using a super-parallel MR microscope operated at 2.34T (Shiota 2007; Matsuda et al., 2003, 2007; Yamada et al., 2006).

In the present study, the precise external morphology and morphometry of the embryonic liver was studied using MR imaging data of human embryos from the Kyoto Collection of Human Embryos (http://bird.cac.med.kyoto-u.ac.jp). These data will serve as a useful reference for evaluating the development of the embryonic liver and adjacent organs and how they morphologically affect each other.

MATERIALS AND METHODS

Human Embryo Specimens

Approximately 44,000 human embryos, comprising the "Kyoto collection," are historical specimens collected and stored at the Congenital Anomaly Research Center of Kyoto University (Nishimura et al., 1968; Nishimura, 1975; Shiota, 1991; Yamada et al., 2004). In most cases, pregnancy was terminated during the first trimester of pregnancy for socioeconomic reasons under the Maternity Protection Law of Japan. Some of the specimens (~20%) are undamaged, well-preserved embryos. When the aborted materials were brought to the laboratory, the embryos were measured, examined, and staged using the criteria of O'Rahilly and Müller (1987). Approximately 1,200 well-preserved human embryos diagnosed as externally normal at CS13 to CS23 were selected for MR microscopic imaging. The conditions used to acquire the MR images of the embryos are described elsewhere (Shiota, 2007; Matsuda et al., 2003, 2007; Yamada et al., 2010).

MR Image Processing and Selection of the Datasets

3D MR image datasets for each embryo were initially obtained from 256 × 256 × 512 voxels. Each dataset was first converted into a two-dimensional (2D) stack and saved as an audio video interleave (.avi) file format using software ImageJ™ (version1.42q, National Institutes of Health, Bethesda, MD). Sequential 2D images were resectioned digitally and 3D images were reconstructed using the software OsiriX™ (version 3.7.1, Pixmeo SARL, Geneva, Switzerland). Both 2D and 3D images were carefully observed and selected according the following conditions: (1) no obvious damage or significant anomaly present in the external appearance, (2) body axes maintained in the original form that is not deformed artificially during fixation and preservation, (3) sufficiently high quality of reconstructed 2D images to properly extract the organs and tissues, and (4) liver, stomach, IVC located in the normal anatomic position.

For the present study, 67 samples were selected from the 1,200 MR image datasets based on the criteria described earlier, consisting of five cases each for CS14, CS16, CS18, CS19, CS21, and CS22; nine cases each for CS15, CS20, and CS23; and 10 cases for CS17.

3D Reconstruction of the Liver and Adjacent Organs

The avi file format images obtained from 3D MR images were resectioned digitally to the suitable planes for each analysis using the multiplanar reformatting tool in software Image J and OsiriX. Targeted organs of interest were segmented in a series of coronal-sectional images using the region of interest (ROI) module in OsiriX. 3D objects were computationally reconstructed with DeltaViewer™ (http://delta.math.sci.osaka-u.ac.jp/DeltaViewer/index-j.html; Yamada et al., 2007). Morphogenesis of the liver and adjacent organs was analyzed in detail using the 3D images (see Supporting Information Video S1, S2, S3).

Measurements of the Liver

For accurate anatomic assignment of the cranial/caudal (Z), left/right (X), and dorsal/ventral (Y) axes, the cranial/caudal axis of the liver was first determined using OsiriX. The z-axis was defined as the line that goes through the most cranial and caudal neural tubes in a series of coronal-section images that include the liver (Fig. 1A). The orthogonal plane of the z-axis was then determined and the x- and y-axes were defined as shown in Fig. 1B. Lengths of the liver along each axis

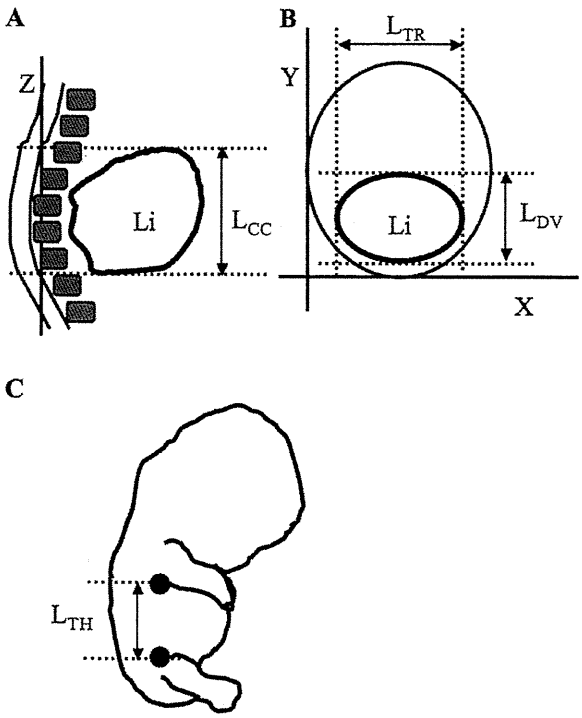

Fig. 1. Morphometry of the liver (**A**,**B**) An orthogonal coordinate system was defined using craniocaudal (Z)-axis, left/right (X)-axis, and dorsoventral (Y)-axis as described in the Materials and Methods section. Length of the liver along each axis was defined as craniocaudal length (L_{CC}) transverse length (L_{TR}), and dorsoventral length (L_{DV}), respectively. Li; liver (**C**) Trunk height (L_{TH}), the length between the axilla and the cranial end of the trochanterion (●),was used to measure the change in the crania-caudal growth of the abdominal cavity using the method of Otani et al. (2008) with some modification.

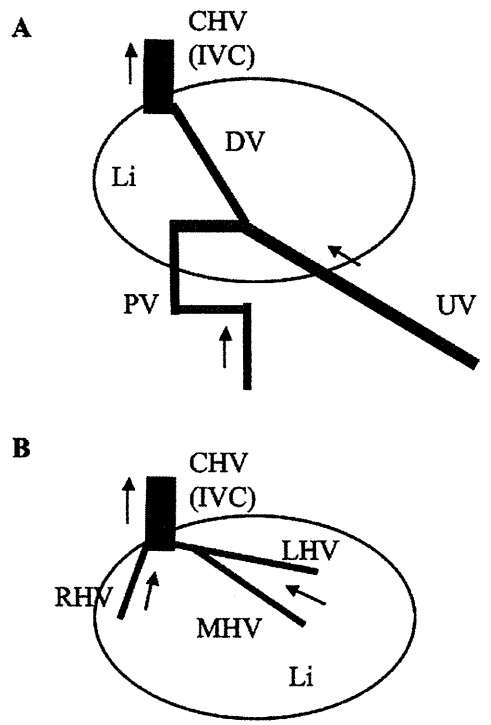

Fig. 2. Schematic representation of embryonic circulation of the liver. (**A**) Definitive afferent venous circulation of the asymmetrical stage (**B**) Definitive efferent venous vessels. Arrow indicates the direction of venous flow. Li, liver; DV, ductus venosus; PV, portal vein; UV, umbilical vein; CHV, common hepatic vein; IVC, inferior vena cava; RHV, right hepatic vein; LHV, left hepatic vein; MHV, middle hepatic vein.

were defined as the transverse length (L_{TR}), dorsoventral length (L_{DV}), and craniocaudal length (L_{CC}) (Fig. 1A,B).

The liver was extracted from a series of coronal-section images as described above. The volume of the liver was calculated by stacking the extracted liver in a series of coronal-section images using the ROI module of OsiriX. The volume of the embryo was calculated using the Region Growing module in OsiriX.

We measured trunk height (L_{TH}) as the change in the craniocaudal growth of the abdominal cavity according to a previous study by Otani et al. (2008) with some modification (Fig. 1C). In the present article, the axilla was marked instead of the acromion used by Otani et al. (2008), because the axilla was more evident on our 3D images.

Estimation of Vascular Architecture in the Liver

To elucidate the asymmetry of the afferent venous vessels, the following four vessels were reconstructed three-dimensionally; the ductus venosus, umbilical vein, portal vein, and common HV (Fig. 2A). The common HV becomes the intrahepatic part of the IVC in later stages. The three efferent venous vessels, the right, left, and middle HVs (Fig. 2B), were also estimated on 2D serially sectioned images.

RESULTS

Anatomic Relationships with the Liver

The morphogenesis of the liver was affected by the development of adjacent organs and tissues, such as the heart, diaphragm, stomach, umbilicus, abdominal wall, and adrenal gland. To elucidate the characteristic changes occurring stage- and organ-specifically, the morphogenesis of the liver is described in detail in relation to the development of adjacent organs and tissues.

Intrathoracic Organs

The right and left ventricles were at the same level along the cranial/caudal axis, and the liver was in contact with the ventricles at CS15 in the 2D image. As a consequence, the liver formed a prominence on the bilateral cranial region in all 11 cases at CS15 and CS16 (Fig. 3A-a,b). From CS17, the left ventricle developed to the left medial-caudal side, which resulted in the formation of an obvious depression in the left medial cranial region and prominences bilaterally on the cranial surface of the liver in all 11 cases (100%) between CS17 and CS19 (Fig. 3A-c,d). This depression in the left medial cranial region is a characteristic temporal feature of the

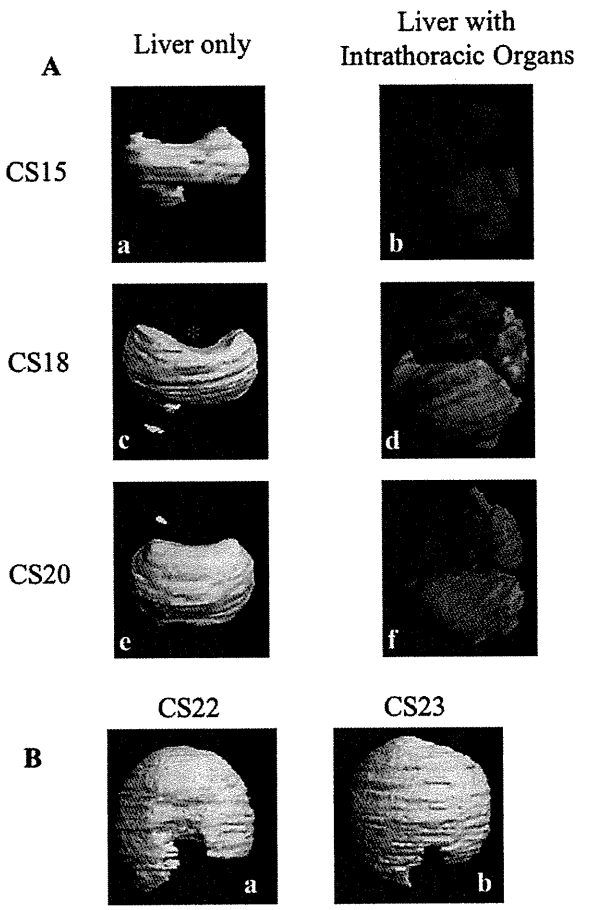

Fig. 3. Representative 3D image of the embryonic liver, demonstrating the anatomic relationship between the intrathoracic organs and the liver. (**A**) Ventral and left lateral view of the liver by 3D image between CS15 and CS20. The liver (green), lung (blue), and heart (red) were reconstructed in the picture (b, d, f). The depression formed by the left ventricle (*) is a characteristic temporal feature of the cranial surface of the liver between CS17 and CS19. (**B**) Ventral view of the liver by 3D image at CS22 and CS23. A prominence was formed in the central region of the cranial surface of the liver at CS22. The top of this prominence moved toward the right at CS23. The prominence formed by the left ventricle is a characteristic temporal feature of the cranial region of the liver at CS22 and CS23.

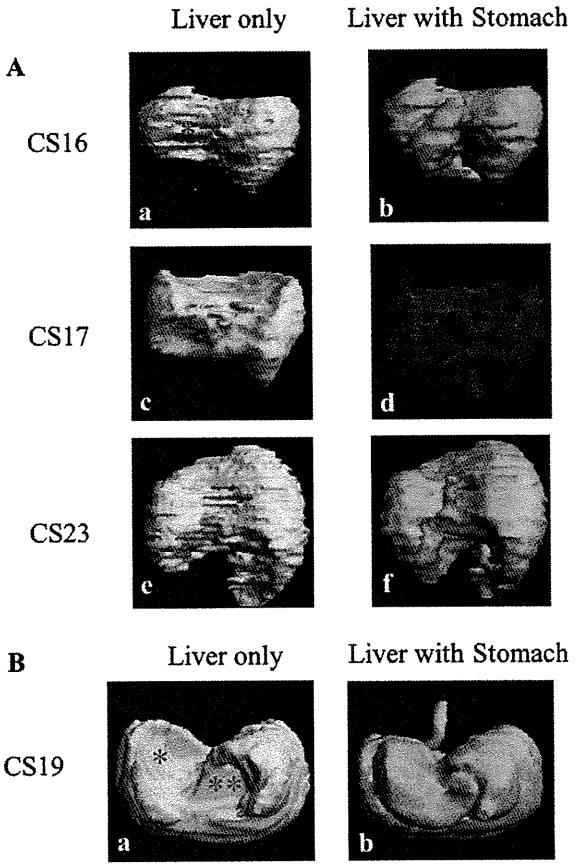

Fig. 4. Representative 3D image of the embryonic liver, demonstrating the anatomic relationship between the stomach and liver. (**A**) Dorsal view of the liver by 3D image between CS16 and CS23 The liver (green) and stomach (orange) was reconstructed (b, d, f). The "Imprint of the stomach" (*) changed according to the morphogenesis of the stomach and become deeper until CS23. (**B**) Caudal view of the liver by 3D image showing the "imprint of the stomach" (*) and "horizontal plane by pyloric-antrum" (**).

liver between CS17 and 19, and is hence termed the "heart depression." The "heart depression" was deep (maximum) until CS18, and then disappeared in 4 of 8 cases (50%) at CS20 and in 17 of 18 cases (94.4%) after CS21 (Fig. 3A-e,f). Next, the liver formed a prominence in the central region of the cranial surface in all 5 cases at CS22, as the thickness of the diaphragm was sufficiently developed to create a distinct border between the thoracic and abdominal cavities (Fig. 3B-a). The top of this prominence moved toward to the right in 7 of 8 cases (87.5%) at CS23, while the left ventricle developed left-ventrally (Fig. 3B-b).

The lung was recognized from CS14, and was in close contact with the dorsal side of the liver between CS14 and CS18 (Fig. 3A-b,d). The lung and liver were clearly separated by the developing diaphragm after CS19 in all 31 cases (Fig. 3A-f). The lung did not seem to affect the morphogenesis of the liver during development.

Stomach

The liver was deformed on the dorsal and caudal surface because of the organogenesis of the upper digestive tract, especially the stomach. The stomach formed hollows on the left-medial regions of the dorsal surface of the liver, that developed a fusiform in all 6 cases at CS15 (Fig. 4A-a,b). Then, the liver developed by covering the stomach along the greater curvature, while the stomach formed a greater and lesser curvature and rotated around in a 3D manner. As a consequence, the oral side of the stomach formed hollows on the dorsal-caudal surface of the liver in all 5 cases at CS18 (Fig. 4A-c,d). As the stomach rotated, the anal side of the stomach formed a loop, which became the pyloric

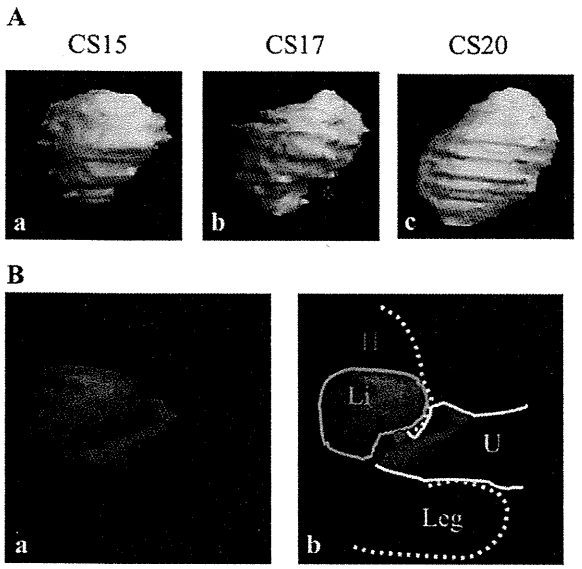

Fig. 5. Anatomic relationship between the umbilicus and liver (**A**) Representative right lateral view of the liver by 3D image between CS15 and CS20 showing the "depression by umbilicus" (*). This depression is a characteristic temporal feature at the abdominal region of the liver between CS16 and CS19. (**B**) Lateral view of the liver by 3D image at CS17 showing the relationship between the liver (Li; green) and umbilicus (U; yellow). External form of umbilicus, leg, and chest-abdominal wall is represented by the yellow and dashed lines, respectively. Red and blue circles indicate the entrances to the umbilical vein and intestinal tract, respectively.

antrum. The liver formed a "horizontal plane" by the loop on the caudal surface after CS19 in 27 of 29 cases (Fig. 4B-a,b). Marked hollows formed on the liver with development, such as the "imprint of the stomach" on the caudal surface in all 8 cases at CS23 (Fig. 4A-e,f).

Umbilicus

The part of the liver is in contact with the abdominal wall curved smoothly. The liver looked like a sector from the lateral view in 5 of 6 cases (83.3%) at CS15 (Fig. 5A-a). The liver developed along the cranial-caudal axis, and a depression formed on the ventral-medial region in all 8 cases between CS17 and CS18 (Fig. 5A-b). This depression results from the entry of the umbilical vein and intestinal tract, which herniates physiologically into the umbilical cord (Fig. 5B-a,b). The depression caused by the umbilicus disappeared in all 26 cases after CS20 because the umbilical cord moved toward the caudal side of the abdomen. Flexure of the abdomen of the embryo was evident after CS20. As a consequence, the liver looked like a quadrangle from the lateral view (Fig. 5A-c).

Retroperitoneal Organs

Retroperitoneal organs were located close to the dorsal-caudal side of the liver, but only the right adrenal gland directly contacted the liver. The adrenal gland developed remarkably up to CS19, with the right adrenal gland forming an indentation in the liver (Fig. 6A,B)

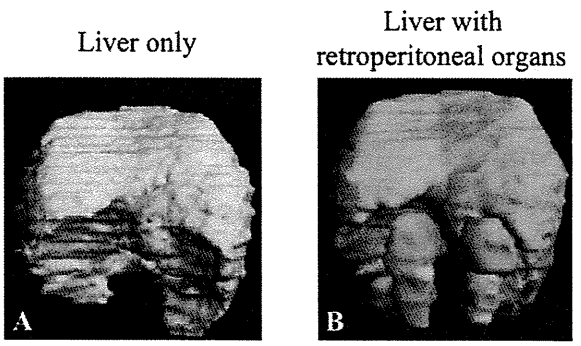

Fig. 6. Dorsal view of the 3D image of the liver at CS22 showing the anatomic relationship between the retroperitoneal organs and the liver. The liver (green), bilateral adrenal gland (purple), metanephros (yellow), and the gonads (brown) were reconstructed (B). The right adrenal gland impinged on the liver, creating an indentation (*), while the left adrenal gland remained separated from the liver by the stomach between them.

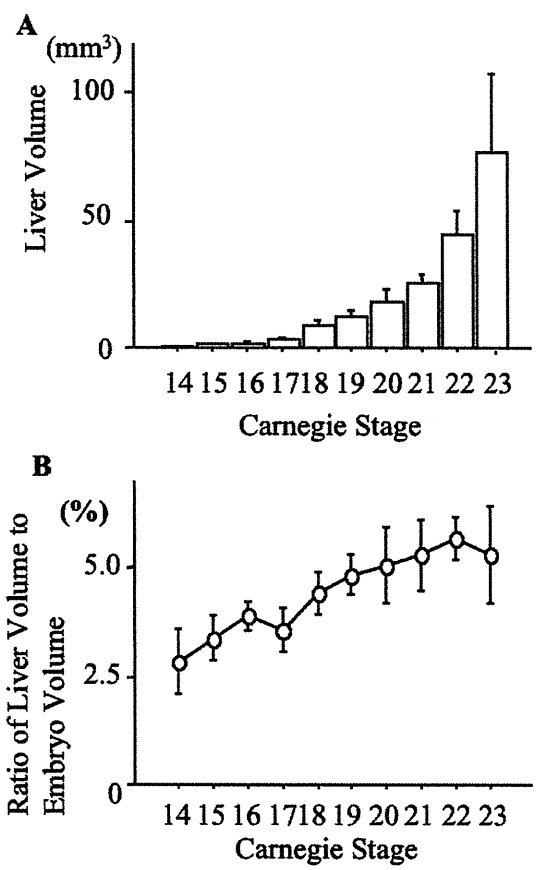

Fig. 7. Calculated liver volume of embryo from CS14 to CS23 (**A**) Liver volume was calculated as described in Materials and Methods section. Data at each CS is shown as mean ± SD mm^3 (**B**) Ratio of liver and embryo (vol/vol %). Whole embryonic volume was calculated as described in the Materials and Methods section. Data at each CS are shown as mean ± SD (%).

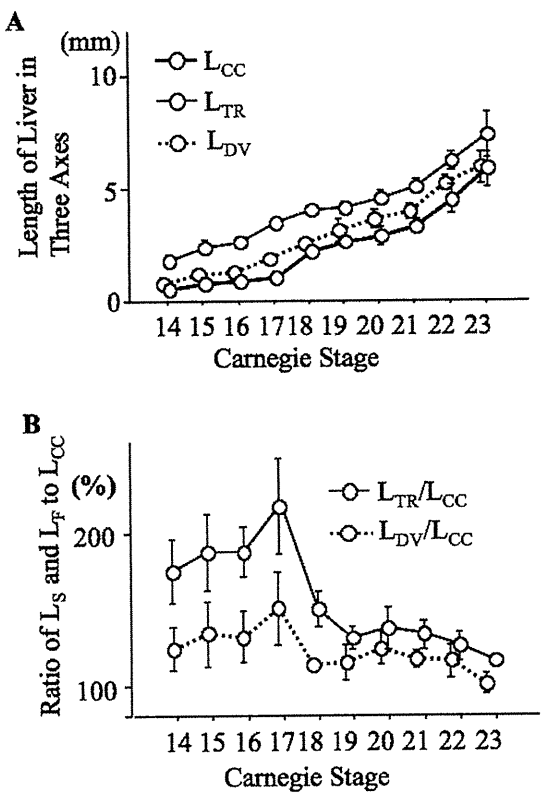

Fig. 8. Morphometry indicating the 3D direction of liver growth (**A**) Change in liver length measured along three axes between CS14 and CS23 (**B**) Ratio of transverse and dorsoventral length (L_{TR}, L_{DV}) to coronal craniocaudal length (L_{CC}) between CS14 and CS23.

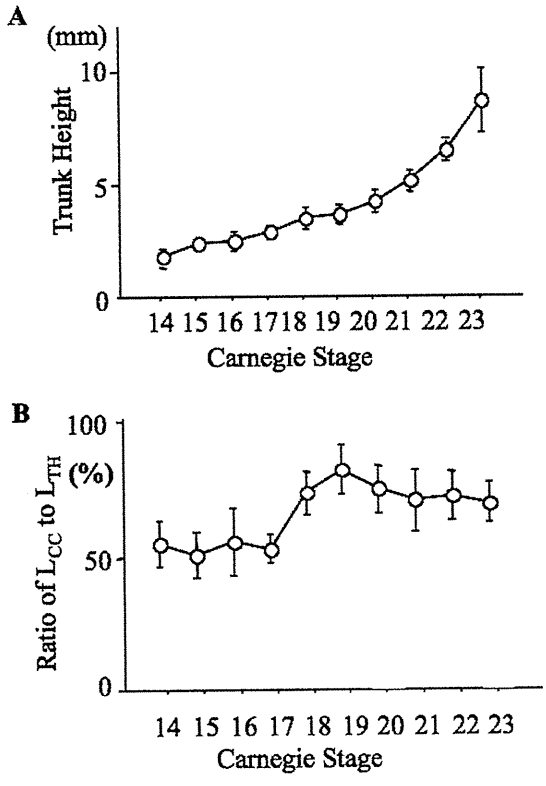

Fig. 9. Trunk height (L_{TH}) (**A**), and ratio of L_{TH} and craniocaudal length (L_{CC}) (**B**) during CS14 and CS23 embryos Trunk height (L_{TH}) was measured as a change in the crania-caudal growth of the abdominal cavity as described in the Materials and Methods section.

in 3 of 5 cases (60%) at CS19 and in all 26 cases after CS20 in the dorsal-caudal region. The indentation formed by the adrenal gland on the liver was unilateral, only on the right side, mainly because the left adrenal gland was separated from the liver by the stomach (Fig. 6A,B). The metanephros and gonads were recognized on MR images after CS21, and seemed to contact the liver. The metanephros and gonads, however, did not seem to affect the morphogenesis of the liver in any of the 18 cases after CS21 (Fig. 6A,B).

Morphometry of the Liver

At CS14, the mean volume of the liver was 0.85 ± 0.32 mm^3 (mean ± SD) and by CS23 it had increased to 77.40 ± 31.30 mm^3 (Fig. 7A). The mean volume of the whole embryo at CS14 was 29.90 ± 7.53 mm^3, and at CS23 it had reached 1458.40 ± 433.60 mm^3. The ratio of liver volume to whole embryonic volume was 2.8 ± 0.8% at CS14, gradually increasing to 5.7 ± 0.5% at CS22 (Fig. 7B).

The length of the liver along the three axes increased exponentially, as shown in Fig. 8A. To clarify the direction of the growth of liver, the ratio of L_{TR} and L_{DV} to L_{CC} according to CS was calculated. The data revealed that the direction of the increase changed at around CS17 and CS19 (Fig. 8B). That is, the liver developed preferentially along the dorso/ventral axis and right/left axis until CS17, along the cranio/caudal axis between CS17 and CS19, and then in all directions after CS19.

L_{TH} increased from 1.84 ± 0.34 mm at CS14 to 8.68 ± 1.40 mm at CS 23 (Fig. 9A). The ratio of L_{CC} to L_{TH} was around 50% between CS14 and CS17, and then it increased to around 75% between CS18 and CS23 (Fig. 9B). The data indicated that the liver occupied about half of the abdominal cavity at CS14 and CS17, and about three-fourths of the abdominal cavity after CS18.

Vascular Architecture of the Liver

Of 62 cases from CS14 to CS23, 61 were defined as asymmetrical. The umbilical vein, portal vein, ductus venosus, and IVC were recognized in each embryo. Primary right and left HVs emerging symmetrically were identified in only one exceptional case.

The arrangement of the three terminal HVs was examined in 62 cases between CS14 and CS23 (Table 1). No HVs were identified in any of the 5 cases at CS14. All the right, left, and medial HVs were recognized between CS15 and CS23 in 39 of 57 cases (68.4%). The remaining 18 cases varied as follows: right and left HV (8 cases, 14.0%), right HV alone (1 case, 1.8%), left and

TABLE 1. Acquisition of three hepatic veins from carnegie stage 14–23

Terminal hepatic vein			Carnegie stage									
Right	Left	Middle	14	15	16	17	18	19	20	21	22	23	No. of total cases
y	y	y	0	1	2	6	4	5	7	4	4	6	39
y	y	–	0	5	2	0	1	0	0	0	0	0	8
y	–	–	0	0	0	0	0	0	0	0	0	1	1
–	y	y	0	0	1	1	0	0	1	1	1	0	5
–	y	–	0	1	0	1	0	0	0	0	0	1	3
–	–	y	0	0	0	0	0	0	0	0	0	0	0
–	–	–	5	1	0	0	0	0	0	0	0	0	6
No. of total cases			5	8	5	8	5	5	8	5	5	8	62

Acquisition of right, left, and middle hepatic veins is indicated as "y".
Five of 67 cases were unfit for estimation of vascular architecture.

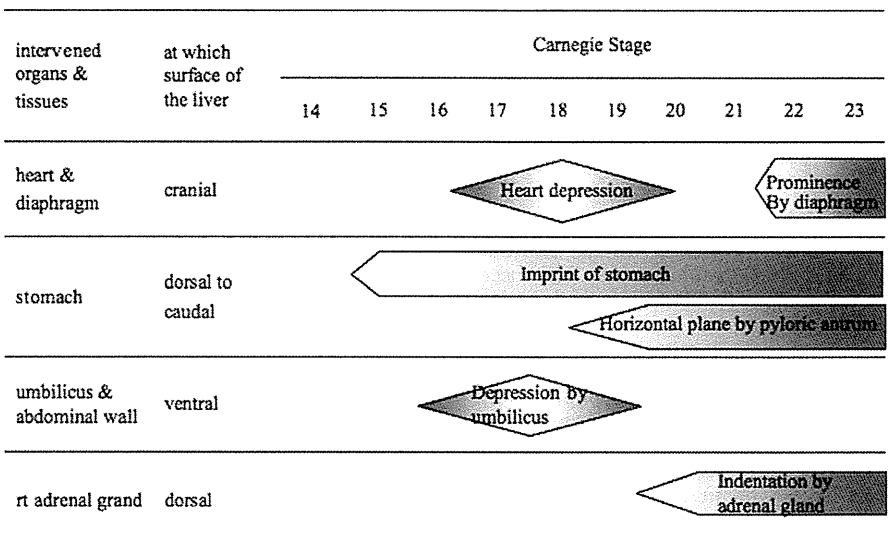

Fig. 10. Development of adjacent organs and tissues that may affect liver morphogenesis. Temporal (stage-specific) and organ-specific effects are indicated and named according to the Carnegie stage.

middle HV (5 cases, 8.7%), left HV alone (3 cases, 5.3%), and no HV (1 case, 1.8%).

DISCUSSION

The liver bud grows rapidly, and the embryonic liver occupies most of the abdominal cavity after the end of the 6th gestational week (ca. CS16; Hutchins and Moore, 1988; Lemaigre, 2009). The details of the morphologic and morphometric features of the liver during the early embryonic period, however, have remained unknown. Mall (1906) made wax models of the liver exterior from serial histologic sections of the human embryo to study the positional relationship of the gall bladder and vascular system from an outside view. He only described the morphologic changes of the liver in embryos between 17.5 and 24 mm in size; "By comparing the livers of three embryos it is seen that only their upper surfaces are regular in form from stage to stage; the processes extending into the abdominal cavity are irregular, to fit into the spaces that there are for them to grow into." Severn (1971) examined serial histologic sections of 38 human embryos from CS9 through CS11. For his detailed histologic observation, 3D drawings of the developing foregut and hepatic diverticulum were made, showing the change in the external appearance. Hutchins and Moore (1988) reported that the liver appeared at CS11 and grew to over 90 mm^3 in volume by CS23. They calculated the difference in the volume between right- and left-halves of the liver, divided by the median sagittal plane; the right half was large with an average proportion of 57.8%, and the ratio was almost constant in all embryos from CS11 through CS23. In the present study, external morphologic and morphometric analysis of the liver during embryonic periods was performed using MR imaging data acquired from embryos obtained from the Kyoto Collection. The present data revealed a unique external morphology as well as the quantitative morphometry of the embryonic liver.

Morphogenesis of the liver was strongly affected by the adjacent organs and tissues. The characteristic effects of stage- and organ-specific changes are summarized in Fig. 10. The left ventricle developed to the left medial-caudal side, which resulted in the formation of a clear depression in the left medial region and prominence bilaterally on the cranial surface of the liver between CS17 and CS19 (Fig. 3A-c,d). An imprint of the stomach formed at the

dorsal left-medial region of the liver, and became more marked with development until CS23 (Fig. 4A-a,c,e). A depression caused by the umbilicus formed in the ventral region of the liver between CS16 and CS19 (Fig. 5A-b). An indentation created by the right adrenal gland was formed at the dorsal-caudal region of the liver surface from CS20 (Fig. 6-a,b). Therefore, the morphology of the embryonic liver reflects the development of the adjacent organs during organogenesis.

Morphometric analysis in the present study revealed that the volume of the liver increased exponentially from CS14 through CS23, and the ratio of L_{TR}, L_{DV}, and L_{TH} to L_{CC} presented here indicated that the direction of growth changed at around CS17 and CS19 (Figs. 8B, 9B). That is, the liver developed preferentially along the dorso/ventral axis and right/left axis until CS17, along the cranio/caudal axis between CS17 and CS19, and then in all three directions. The occurrence of several important developmental phenomena around CS17 may affect the morphometric data (O'Rahilly and Müller, 1987; Moore, 2008; Schoenwolf and Larsen, 2009). When the septum transversum begins to differentiate into the diaphragm, development in the cranial direction is limited, while development towards the abdominal cavity is accelerated likely due to extension of the body axis of the embryo and physiologic herniation of the intestine into the umbilical cord, which creates space and transform the inner structures of the abdominal cavity (O'Rahilly and Müller, 1987).

Original and first-hand data regarding the stages of development of the vascular architecture of the liver are scarce (Collardeau-Frachon and Scoazec, 2008). Though the asymmetry of the hepatic vascular structure may be acquired between CS13 and CS16, the precise stages of development could not be determined. The right umbilical vein, which is an important indicator of the symmetrical stage, was clearly detected at CS13 (O'Rahilly and Müller, 1987). In the present study, only one case showed the right umbilical vein at CS14 and other 61 of 62 cases had already lost the right umbilical vein by CS14; that is, the hepatic vascular structure was already asymmetrical. The present data suggest that the fundamental architecture of the asymmetrical stage is acquired between CS13 and CS14 in almost embryos.

The terminal HVs formed at a similar stage as the afferent circulation system, as mentioned earlier. In the present study, three HVs were observed in 68.4% of the cases after CS15, indicating that the three HVs are acquired around CS15 in most cases. These data are consistent with those of a previous study reporting profound remodeling of the efferent venous system during the 5th gestational week (Dickson, 1957; Collardeau-Frachon and Scoazec, 2008). Three HVs were not identified until after CS17 in 19.6% of cases, suggesting that there are several individual variations in the number and arrangement of the terminal HVs, in contrast to the afferent venous circulation systems. It is so far impossible to distinguish an anomaly from a variation in individual embryos, mainly because only terminal HVs were detected on the MR image. Detailed identification of such a small branch of the vessels depends on the resolution of the imaging technique. Further improvements in imaging modalities are expected that will allow for more precise detection of the intrahepatic vascular system and application to analyses at CS13 or earlier.

Recent advances in medical imaging allow for earlier assessment of human development and prenatal diagnosis in the first trimester. Data about normal development during the embryonic stages, however, remain inadequate for guiding such clinical evaluations. Insights into the dynamic and complex processes during organogenesis will require accurate morphologic data with dynamic modeling of embryonic structures. Furthermore, 3D reconstructions are necessary to elucidate the complex anatomic remodeling that occurs during these early embryonic stages. From this point of view, the present data will be useful for evaluating the appropriate development of the embryonic liver based on the external morphology, and for evaluating adjacent organs that affect the morphology of the liver stage-specifically. This information will be an indispensable reference for clinical evaluation with obstetrical ultrasonography in the early gestational weeks, which will be useful for fetal medicine and prenatal diagnosis.

ACKNOWLEDGEMENTS

We are deeply indebted to Executive Vice President of Kyoto University, Kohei Shiota, for providing the invaluable MR data. We also acknowledge the contribution of collaborating obstetricians and the previous members of the Congenital Anomaly Research Center, Kyoto University Graduate School of Medicine.

LITERATURE CITED

Bone SN, Johnson GA, Thompson MB. 1986. Three-dimensional magnetic resonance microscopy of the developing chick embryo. Invest Radiol 21:782–787.

Carlson BM. 2009. Digestive and respiratory systems and body cavities, cardiovascular system. In: Human embryology and developmental biology. 2nd ed. Philadelphia: Mosby, Elsevier. p 353–392, 429–476.

Collardeau-Frachon S, Scoazec JY. 2008. Vascular development and differentiation during human liver organogenesis. Anat Rec 291:614–627.

Couinaud C. 1996. Translation and adaptation. 1st English ed. Surgical Anatomy of the Liver Revisited. 1st Japanese ed. Tokyo: Igaku-Shoin.

Dickson AD. 1957. The development of the ductus venosus in man and the goat. J Anat 91:358–368.

Drews U. 1995. Gastrointestinal tract. In: Color atlas of embryology. New York: Thieme Medical.

Effmann EL, Johnson GA, Smith BR, Talbott GA, Cofer G. 1988. Magnetic resonance microscopy of chick embryos in vivo. Teratology 38:59–65.

Haishi T, Uematsu T, Matsuda Y, Kose K. 2001. Development of a 1.0 T MR microscope using a Nd-Fe-B permanent magnet. Magn Reson Imaging 19:875–880.

Hutchins GM, Moore GW. 1988. Growth and asymmetry of the human liver during the embryonic period. Pediatr Pathol 8:17–24.

Lemaigre FP. 2009. Mechanisms of liver development: concepts for understanding liver disorders and design of novel therapies. Gastroenterology 137:62–79.

Mall FP. 1906. A study of structural unit of the liver. Am J Anat 5:227–308.

Matsuda Y, Utsuzawa S, Kurimoto K, Haishi T, Yamazaki Y, Kose K, Anno I, Marutani M. 2003. Super-parallel MR microscope. Magn Reson Med 50:183–189.

Matsuda Y, Utsuzawa S, Kurimoto T, Haishi T, Yamazaki Y, Kose K, Anno I, Marutani M. 2007. Imaging of a large collection of human embryo using a super-parallel MR microscope. Magn Reson Med Sci 6:139–146.

Moore KL. 2008. The digestive system. In: The developing human: clinically oriented embryology. 8th ed. Philadelphia: Saunders. p 211–242.

Nishimura H, Takano K, Tanimura T, Yasuda M. 1968. Normal and abnormal development of human embryos: first report of the analysis of 1213 intact embryos. Teratology 1:281–290.

Nishimura H. 1975. Prenatal versus postnatal malformations based on the Japanese experience on induced abortions in the human being. In: Blandau RJ, editor. Aging gametes. Basel: S Karger AG. p 349–368.

Otani H, Udagawa J, Lundh T, Hatta T, Hashimoto R, Matsumoto A, Satow F. 2008. Morphometric study on the characteristic external features of normal and abnormal human embryos. Congenit Anom (Kyoto) 48:18–28.

O'Rahilly R, Müller F. 1987. Developmental stages in human embryos: including a revision of Streeter 's "horizons" and a survey of the carnegie collection. Washington, DC: Carnegie Institution.

Sadler TW, Langman J. 2010. Cardiovascular system, digestive system. In: Langman's medical embryology. 11th ed. Philadelphia: Walters Kluwer Health, Lippincott William & Wilkins. p 165–200, 209–234.

Schoenwolf GC, Larsen WJ. 2009. Development of the gastrointestinal tract. In: Larsen's human embryology. 4th ed. Philadelphia: Churchill Livingstone: Elsevier. p 435–477.

Severn CB. 1971. A morphological study of the development of the human liver. I. Development of the hepatic diverticulum. Am J Anat 131:133–158.

Shiota K. 1991. Development and intrauterine fate of normal and abnormal human conceptuses. Congenit Anom (Kyoto) 31:67–80.

Shiota K, Yamada S, Nakatsu-Komatsu T, Uwabe C, Kose K, Matsuda Y, Haishi T, Mizuta S, Matsuda T. 2007. Visualization of human prenatal development by magnetic resonance imaging (MRI). Am J Med Genet A 143A:3121–3126.

Smith BR, Effmann EL, Johnson GA. 1992. MR microscopy of chick embryo vasculature. J Magn Reson Imaging 2:237–240.

Smith BR, Johnson GA, Groman EV, Linney E. 1994. Magnetic resonance microscopy of mouse embryos. Proc Natl Acad Sci U S A 91:3530–3533.

Smith BR, Linney E, Huff DS, Johnson GA. 1996. Magnetic resonance microscopy of embryos. Comput Med Imaging Graph 20:483–490.

Yamada S, Uwabe C, Fujii S, Shiota K. 2004. Phenotypic variability in human embryonic holoprosencephaly in the Kyoto Collection. Birth defects research. A Clin Mol Teratol 70:495–508.

Yamada S, Uwabe C, Nakatsu-Komatsu T, Minekura Y, Iwakura M, Motoki T, Nishimiya K, Iiyama M, Kakusho K, Minoh M, Mizuta S, Matsuda T, Matsuda Y, Haishi T, Kose K, Fujii S, Shiota K. 2006. Graphic and movie illustrations of human prenatal development and their application to embryological education based on the human embryo specimens in the Kyoto collection. Dev Dyn 235:468–477.

Yamada S, Itoh H, Uwabe C, Fujihara S, Nishibori C, Wada M, Fujii S, Shiota K, 2007. Computerized three-dimensional analysis of the heart and great vessels in normal and holoprosencephalic human embryos. Anat Rec (Hoboken). 290:259–267.

Yamada S, Samtani RR, Lee ES, Lockett E, Uwabe C, Shiota K, Anderson SA, Lo CW. 2010. Developmental atlas of the early first trimester human embryo. Dev Dyn 239:1585–1595.

Congenital Anomalies
THE JAPANESE TERATOLOGY SOCIETY
doi:10.1111/j.1741-4520.2011.00345.x
Congenital Anomalies 2012; **52**, 55–58

SHORT COMMUNICATION

Morphometric analysis of the brain vesicles during the human embryonic period by magnetic resonance microscopic imaging

Takashi Nakashima[1], Ayumi Hirose[1], Shigehito Yamada[2], Chigako Uwabe[2], Katsumi Kose[3], and Tetsuya Takakuwa[1]
[1]Human Health Science and [2]Congenital Anomaly Research Center, Graduate School of Medicine, Kyoto University, Kyoto, and [3]Institute of Applied Physics, University of Tsukuba, Ibaragi, Japan

ABSTRACT **The development of the brain vesicles between Carnegie stages (CS) 17 and 23 was analyzed morphometrically using 177 magnetic resonance image data derived from the Kyoto Collection of Human Embryos. Whole embryonic volume was 106.55 ± 21.08 mm^3 at CS17, exponentially increasing to CS23 when it reached 1357.28 ± 392.20 mm^3. Length of brain vesicles was 29.83 ± 2.52 mm at CS17, increased almost linearly and reached 49.31 ± 6.66 mm at CS23. The rate of increase was approximately 4.2 times higher on the dorsal side than on the ventral side. The increase in the length of the brain vesicles resulted mainly from that of the prosencephalon, and the rate of increase was three times higher on the dorsal side than on the ventral side of the prosencephalon.**

Key Words: brain vesicle, human embryo, magnetic resonance imaging, morphometry, neural tube

INTRODUCTION

Embryonic development is characterized by dynamic and gross changes in the external appearance in accord with internal organogenesis. The Developmental Horizons and Carnegie Stages (CS) (O'Rahilly 1972; O'Rahilly and Müller 1987) are monumental works, both of which are determined by qualitative observation of the external appearance of the human embryo in accord with internal organogenesis. They have been predominantly used as the most reliable indices of human embryonic development. Further, they have been applied to the staging of various vertebrate embryos (Butler and Juurlink 1987).

Additional quantitative data are indispensable for many studies, such as the study of individual differences, symmetry, rate of growth, evaluation of developmental delay due to various causes, and comparisons with other mammalian species. However, quantitative data on the human embryonic period have been limited to measurement from the outside, such as crown–rump length and body weight. Only a few quantitative studies have dealt with the external features of various parts in developing human embryos (Jackson 1909; O'Rahilly and Müller 1984). Recently, Otani et al. (2008) proposed defined measurements of body parts as well as of the whole body, and established a set of approximate standards. These measurements required arduousness and a high degree of skill to minimize errors. Each embryo was set under a dissecting microscope with an attached scale so that the dimension to be measured was parallel to the surface of the scale.

Correspondence: Tetsuya Takakuwa, MD, PhD, Human Health Science, Graduate School of Medicine, Kyoto University, Sakyo-ku Shogoin Kawahara-cyo 53, Kyoto 606-8507, Japan. Email: tez@hs.med.kyoto-u.ac.jp

Received August 19, 2011; revised and accepted October 2, 2011.

Quantitative observation of internal structures has also been difficult because the internal developmental process has been examined mainly using classic histology-based methods with a small number of samples. Recently three-dimensional (3D) imaging techniques have dramatically improved examination methods. With the advent of magnetic resonance (MR) imaging, the imaging of embryos has proven to be highly effectual (Effmann et al. 1988; Smith et al. 1992; Haishi et al. 2001), providing a resolution of 40 μm/pixel or more with long scan times. MR imaging is a non-invasive and non-destructive method that has many possibilities not only for precise morphological observations but also for morphometric evaluations of internal structures.

The human brain is arguably one of the most complicated organs in living systems (O'Rahilly and Müller 2006; Bayer and Altman 2008; Huang et al. 2009). This elaborate structure originates from a simple neural tube, followed by a series of differentiation processes. Morphometric characterization of the brain vesicles at each stage not only aids in understanding this highly ordered developmental process but also provides clues to detecting abnormalities caused by genetic or environmental factors. In this connection, morphometric data of brain vesicles and whole embryo volume using MR data was provided in the present study. Such methods and obtained morphometric data will pave the way for analyzing human embryos.

MATERIALS AND METHODS

Human embryo specimens

Approximately 44 000 human embryos comprising the Kyoto Collection are historical specimens collected and stored at the Congenital Anomaly Research Center of Kyoto University (Nishimura et al. 1968; Nishimura 1975; Shiota 1991; Yamada et al. 2004). In most cases, pregnancy was terminated during the first trimester for socioeconomic reasons under the Maternity Protection Law of Japan. Some of the specimens (~20%) are undamaged, well-preserved embryos. When the aborted materials were brought to the laboratory, the embryos were measured, examined and staged using the criteria of O'Rahilly and Müller (1987). Approximately 1200 well-preserved human embryos diagnosed as externally normal from CS13 to CS23 were selected for MR microscopic imaging. The conditions used to acquire the MR images of the embryos are described elsewhere; Matsuda et al. 2003, 2007; Yamada 2006; Shiota et al. 2007). The present study was approved by the Committee of Medical Ethics of Kyoto University Graduate School of Medicine, Kyoto, Japan (E986).

MR image processing and selection of the datasets

3D MR image datasets for each embryo were initially obtained from 256 × 256 × 512 voxels. Each dataset was first converted into a two-dimensional (2D) stack and saved as an audio video

interleave (.avi) file format using software ImageJ version 1.42q (National Institutes of Health, Bethesda, MD, USA). Sequential 2D images were re-sectioned digitally and 3D images were reconstructed using the software OsiriX version 3.7.1 (Pixmeo SARL, Geneva, Switzerland). Both 2D and 3D images were carefully observed and selected according to the following conditions: (i) no obvious damage or significant anomaly present in the external appearance; (ii) head and neck axes maintained in the original form (i.e. not deformed artificially during fixation and preservation); and (iii) sufficiently high quality of reconstructed 2D images to properly extract the organs and tissues. For the present study, 177 samples distributed between CS17 and 23, consisting of 25 or more samples for each stage, were selected from the 1200 MR image datasets based on the criteria described above.

3D reconstruction of the embryo and morphometry of the brain vesicles

The present study used 3D images reconstructed using the maximum intensity projection (MIP) module in software OsiriX. The projected 3D images gave both external and internal information. The lateral view of the 3D images on the screen were captured using Screenshot Plus version 3.2 (Steven Chaitoff, CA, USA) and measured using the software Photoshop CS4.0 (Adobe Systems Incorporated, CA, USA). Length was measured by pixel on the image on the screen and then converted to millimeters using voxel/pixel and voxel/mm ratios specific for each embryo.

The length of whole neural tube surrounding was measured, and that was divided into the regions of brain vesicles and spinal cord by the level of C1 for the first cervical vertebra (Fig. 1A). The spinal cord region was further subdivided by the line that connects the acromion and trochanter to dissect the region of spinal cord corresponding to the trunk and tail (Fig. 1B).

The brain vesicles after CS18 were divided into the following six regions according to anatomic landmarks (Fig. 1C): ventral region of the prosencephalon (PV) – the length between the olfactory bulb (ob) and the supramammillary recess (sr); dorsal region of the prosencephalon (PD) – the length between the posterior commissure (pc) and ob; ventral region of the mesencephalon (MV) – the length between the supramammillary recess (sr) and the isthmic recess (ir); dorsal region of the mesencephalon (MD) – the length between pc and the isthmic groove (ig); ventral region of the rhombencephalon (RV) – the length between ir and the level of C1; and dorsal region of the rhombencephalon (RD) – the length between ig and the level of C1.

The volume of the embryo was measured using region growing module in OsiriX.

RESULTS AND DISCUSSION

Whole embryonic volume

The whole embryonic volume was 106.55 ± 21.08 mm^3 at CS17, exponentially increasing until CS23 when it reached 1357.28 ± 392.20 mm^3 (Fig. 2A). The present data may be comparable with the estimated volume of embryos in the first trimester ultrasound recently reported: 310 ± 137 mm^3 at seven weeks and 1017 ± 352 mm^3 at eight weeks of gestational age (Rousian et al. 2010), although staging was not applied to that study.

Brain vesicles

Length of the brain vesicles was 29.83 ± 2.52 mm at CS17, increased almost linearly and reached 49.31 ± 6.66 mm at CS23 (Fig. 2B-a). Length of the dorsal side of the brain vesicle was

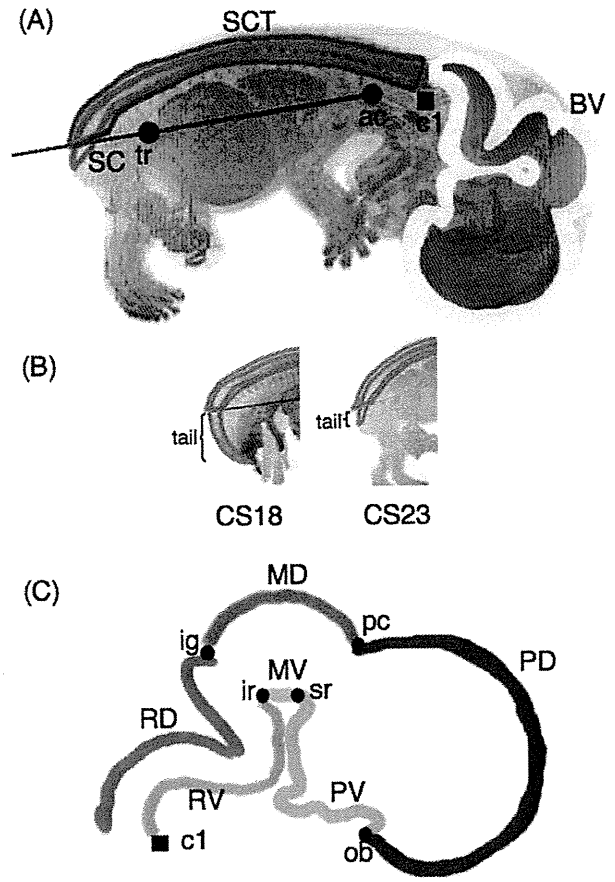

Fig. 1 (A) Lateral view of 3D images reconstructed by maximum intensity projection with drawing showing measurement of brain vesicles. The length of whole neural tube surrounding was measured and divided into the regions of brain vesicles and spinal cord by the level of the first cervical vertebra. The spinal cord was further subdivided by the line that connects the acromion and trochanter to dissect the region of spinal cord corresponding to the trunk and tail. (B) Magnification of spinal cord corresponding to 'tail' region at Carnegie Stage (CS) 18 and CS23. (C) Drawing showing region of the three brain vesicles. Anatomic landmarks for segmentation are indicated: ventral (PV) and dorsal (PD) region of the prosencephalon; ventral (MV) and dorsal (MD) region of the mesencephalon; ventral (RV) and dorsal (RD) region of the rhombencephalon. Ac, acromion; BV, brain vesicles; C1, first cervical vertebra; ig, isthmic groove; ir, isthmic recess; ob, olfactory bulb; pc, posterior commissure; SC, spinal cord; SCT, spinal cord without tail; sr, supramammillary recess; tr, trochanter.

22.85 ± 1.74 mm at CS18, increased linearly and reached 33.38 ± 3.23 mm at CS23 (Fig. 2B-b). While length of the ventral side of the brain vesicle increased only marginally, namely 15.61 ± 1.04 mm at CS18 and 18.11 ± 1.77 mm at CS23, the rate of increase was approximately 4.2 times higher on the dorsal side than on the ventral side.

The dorsal side was analyzed by three primary vesicles: prosencephalon, mesencephalon and rhombencephalon (Fig. 2B-c). Length of the dorsal side of the prosencephalon was 5.65 ± 0.69 mm at CS18, increased linearly and reached 13.75 ± 1.76 mm at CS23. Length of the dorsal side of the mesencephalon was

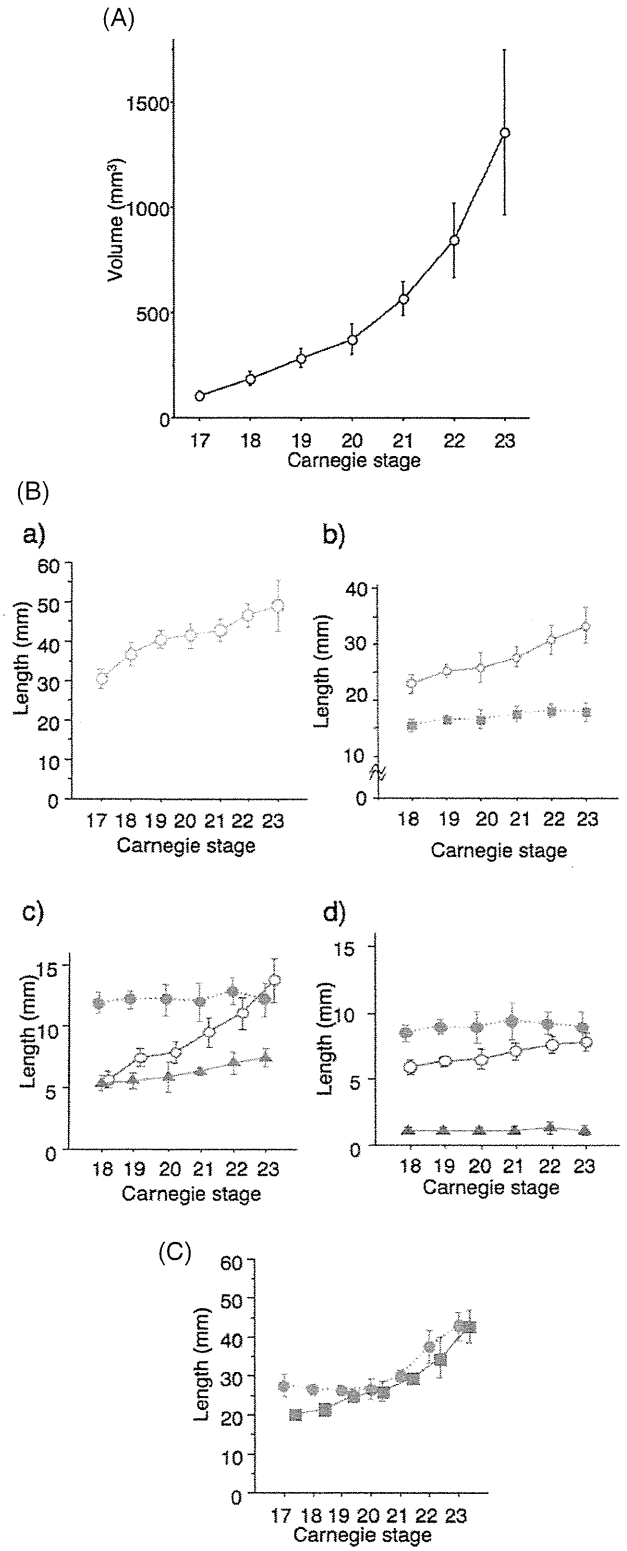

Fig. 2 Morphometry of 3D images from human embryo. (A) Whole embryo volume according to Carnegie stages. (B) Change of length in brain vesicles during development. (a) Change of length in brain vesicles during development. (b) Dorsal (○) and ventral (■) length of brain vesicles during development. (c) Dorsal length of brain vesicles by the regions during development. (○) prosencephalon; (▲) mesencephalon; and (●) rhombencephalon. (d) Ventral length of brain vesicles by the regions during development. (○) prosencephalon; (▲) mesencephalon; and (●) rhombencephalon. (C) Morphometry of spinal cord. Change of length in spinal cord (●) and in spinal cord without tail (■).

5.35 ± 0.62 mm at CS18, increased a little and reached 7.45 ± 0.72 mm at CS23. Length of the dorsal side of the rhombencephalon was almost constant, ranging from 11.85 to 12.86 mm between CS18 and CS23.

The ventral side was also analyzed by the three primary vesicles (Fig. 2B-d). Length of the ventral side of the prosencephalon was 5.66 ± 0.56 mm at CS18, increased linearly and reached 7.88 ± 0.68 mm at CS23. Length of the ventral side of the mesencephalon and the rhombencephalon was almost constant, ranging from 1.22 to 1.43 mm for the former, and from 8.51 to 9.39 for the latter between CS18 and CS23.

The present data revealed that the increase in length of the brain vesicle resulted mainly from that of the prosencephalon, and that the rate of increase was approximately three times higher on the dorsal side than on the ventral side of the prosencephalon.

Spinal cord

Length of the spinal cord was almost constant, ranging from 26.42 to 27.50 mm between CS17 and CS20, then gradually increased and reached 42.82 ± 3.86 mm at CS23 (Fig. 2C). Length of the spinal cord without the tail region (SCT) was 19.88 ± 0.86 mm at CS17, increased gradually and reached 42.59 ± 4.27 mm at CS23.

The difference between spinal cord and SCT, which corresponds to the length of the 'tail region' was 7.62 mm at CS17, and then decreased until CS20, indicating the shortening of the tail region (Fig. 1B). This difference was only between 0.16 and 0.23 mm after CS20.

The present study has demonstrated that analysis using 3D reconstructed images was a useful tool for morphometric evaluations of the internal structures. During morphometric analysis, the projected image was rotated three dimensionally and a lateral image was selected. Then the precise length of the dorsal and ventral lines of the brain vesicles was measured quantitatively, which may reflect the growth of the respective regions. The quantitative data indicate the growth of the respective brain vesicles and spinal cord, as well as dynamic morphogenesis, such as cephalic flexure, cervical flexure and pontine flexure. Morphometric characterization of the brain vesicles at each stage not only aids in understanding this highly ordered developmental process but also provides clues to detecting abnormalities caused by genetic or environmental factors.

ACKNOWLEDGEMENTS

We are deeply indebted to Executive Vice President of Kyoto University, Kohei Shiota, for providing the invaluable MR data. We also acknowledge the contribution of collaborating obstetricians and the previous members of the Congenital Anomaly Research Center, Graduate School of Medicine, Kyoto University. This study was supported by Grant Nos 22591199, 228073, 238058, and 21790180 from Japan Society for the Promotion of Science and BIRD of Japan Science and Technology Agency (JST).

REFERENCES

Bayer SA, Altman J. 2008. The human brain during the early first trimester. London: CRC; Taylor and Francis.

Butler H, Juurlink BHJ. 1987. An atlas for staging mammalian and chick embryos. London: CRC Press.

Effmann EL, Johnson GA, Smith BR, Talbott GA, Cofer G. 1988. Magnetic resonance microscopy of chick embryos in vivo. Teratology 38:59–65.

Haishi T, Uematsu T, Matsuda Y, Kose K. 2001. Development of a 1.0 T MR microscope using a Nd-Fe-B permanent magnet. Magn Reson Imaging 19:875–880.

Huang H, Xue R, Zhang J et al. 2009. Anatomical characterization of human fetal brain development with diffusion tensor magnetic resonance imaging. J Neurosci 29:4263–4273.

Jackson CM. 1909. On the prenatal growth of the human body and the relative growth of the various organs and parts. Am J Anat 9:119–165.

Matsuda Y, Utsuzawa S, Kurimoto K et al. 2003. Super-parallel MR microscope. Magn Reson Med 50:183–189.

Matsuda Y, Utsuzawa S, Kurimoto T et al. 2007. Imaging of a large collection of human embryo using a super-parallel MR microscope. Magn Reson Med Sci 6:139–146.

Nishimura H. 1975. Prenatal versus postnatal malformations based of the Japanese experience on induced abortions in the human being. In: Blandau RJ, editor. Aging gametes. Basel: S. Karger AG. p 349–368.

Nishimura H, Takano K, Tanimura T, Yasuda M. 1968. Normal and abnormal development of human embryos: first report of the analysis of 1213 intact embryos. Teratology 1:281–290.

O'Rahilly R. 1972. Guide to the staging of human embryos. Anat Anz 130S:556–559.

O'Rahilly R, Müller F. 1984. Embryonic length and cerebral landmarks in staged human embryos. Anat Rec 209:265–271.

O'Rahilly R, Müller F. 1987. Developmental stages in human embryos: including a revision of streeter's horizons and a survey of the Carnegie collection. Washington, DC: Carnegie Institution of Washington.

O'Rahilly R, Müller F. 2006. The embryonic human brain: an atlas of developmental stages, 3rd edn. Hoboken: Wiley-Liss.

Otani H, Udagawa J, Lundh T et al. 2008. Morphometric study on the characteristic external features of normal and abnormal human embryos. Congenit Anom (Kyoto) 48:18–28.

Rousian M, Koning AH, van Oppenraaij RH et al. 2010. An innovative virtual reality technique for automated human embryonic volume measurements. Hum Reprod 25:2210–2216.

Shiota K. 1991. Development and intrauterine fate of normal and abnormal human conceptuses. Congenit Anom (Kyoto) 31:67–80.

Shiota K, Yamada S, Nakatsu-Komatsu T et al. 2007. Visualization of human prenatal development by magnetic resonance imaging (MRI). Am J Med Genet A 143:3121–3126.

Smith BR, Effmann EL, Johnson GA. 1992. MR microscopy of chick embryo vasculature. J Magn Reson Imaging 2:237–240.

Yamada S. 2006. Embryonic holoprosencephaly: pathology and phenotypic variability. Congenit Anom (Kyoto) 46:164–171.

Yamada S, Uwabe C, Fujii S, Shiota K. 2004. Phenotypic variability in human embryonic holoprosencephaly in the Kyoto Collection. Birth Defects Res A Clin Mol Teratol 70:495–508.

Kagurasho et al. Head & Face Medicine 2012, 8:2
http://www.head-face-med.com/content/8/1/2

HEAD & FACE MEDICINE

RESEARCH Open Access

Movement of the external ear in human embryo

Miho Kagurasho[1], Shigehito Yamada[2], Chigako Uwabe[2], Katsumi Kose[3] and Tetsuya Takakuwa[1*]

Abstract

Introduction: External ears, one of the major face components, show an interesting movement during craniofacial morphogenesis in human embryo. The present study was performed to see if movement of the external ears in a human embryo could be explained by differential growth.

Methods: In all, 171 samples between Carnegie stage (CS) 17 and CS 23 were selected from MR image datasets of human embryos obtained from the Kyoto Collection of Human Embryos. The three-dimensional absolute position of 13 representative anatomical landmarks, including external and internal ears, from MRI data was traced to evaluate the movement between the different stages with identical magnification. Two different sets of reference axes were selected for evaluation and comparison of the movements.

Results: When the pituitary gland and the first cervical vertebra were selected as a reference axis, the 13 anatomical landmarks of the face spread out within the same region as the embryo enlarged and changed shape. The external ear did move mainly laterally, but not cranially. The distance between the external and internal ear stayed approximately constant. Three-dimensionally, the external ear located in the caudal ventral parts of the internal ear in CS 17, moved mainly laterally until CS 23. When surface landmarks eyes and mouth were selected as a reference axis, external ears moved from the caudal lateral ventral region to the position between eyes and mouth during development.

Conclusion: The results indicate that movement of all anatomical landmarks, including external and internal ears, can be explained by differential growth. Also, when the external ear is recognized as one of the facial landmarks and having a relative position to other landmarks such as the eyes and mouth, the external ears seem to move cranially.

Keywords: External ear, Internal ear, Three-dimensional kinetics, Human embryo, MR imaging

Introduction

External ears, one of the major face components, show an interesting movement during craniofacial morphogenesis in human embryo. The external ear is evidently recognizable after Carnegie stage (CS) 16, and its movement has been described in most embryology textbooks as well [1-5]. The external ears are contained in the lower neck region at CS 17. With the development of the face structure, they ascend to the side of the head at the level of the eyes [6-10]. Streeter [11] has described the essential and precise external movement. The two auricular areas nearly meet in the mid-ventral region in a 6 mm-embryo; they are gradually moved laterally and dorsally. Streeter suggested that the movement of the external ear might be relative rather than real because the external ear is located at the side of the mouth during the development. In the recent study, Gasser [12] proposed that positional changes of the developing structures could be explained by differential growth (i.e. changes in the size and shape of the embryo and its parts) rather than migration (i.e. structures moving from one region of the embryo to another). Gasser demonstrated the evidence by showing the following three examples: sclerotome formation from the somite, spinal ganglion formation from the neural crest, and thymus, thyroid and parathyroid gland formations from pharyngeal endoderm. He emphasized the use of more centralized and less mobile reference points and comparison of both external and internal structures together in the identical magnification for better understanding of the positional changes of the developing structures.

* Correspondence: tez@hs.med.kyoto-u.ac.jp
[1]Human Health Science, Graduate School of Medicine, Kyoto University, 606-8507, Sakyo-ku Shogoin Kawahara-cyo 53, Kyoto, Japan
Full list of author information is available at the end of the article